J Therm Spray Tech (2025) 34:88–96
https://doi.org/10.1007/s11666-025-01938-0

ORIGINAL RESEARCH ARTICLE

Heating Behavior of Cold Spray Particles in Laser

Wanqing Wang[1] · Xinyu Ye[1] · Chengjie Ge[1] · Shuo Yin[2] · Wenya Li[3] · Xinkun Suo[1]

Submitted: 30 September 2024 / in revised form: 15 December 2024 / Accepted: 20 December 2024 / Published online: 24 January 2025

Abstract Laser-assisted cold spraying (LACS) is garnering significant interest as an innovative surface treatment technology that integrates cold spray technology with laser. However, the primary role of laser on in-flight particles remains underexplored. This study aims to elucidate the impact of laser on in-flight particles through meticulously designed experiments and comprehensive multi-physical field simulations, in which the in-flight iron and nickel particles were heated by the laser parallel to the substrates and deposited on the substrates, while the substrates were not heated by the laser. The cross-sectional microstructures, porosity, oxygen content and microhardness of the coatings were characterized to assess the effect of the laser on the in-flight particles. The heating behavior of the in-flight particles under varying velocity and laser power was evaluated using multi-physical field simulations. The results indicated that the microstructures and properties of the coatings, including porosity, flattening ratios, oxygen content and microhardness, were not significantly influenced by the laser irradiation. The simulations further revealed that the laser irradiation had negligible effect on the temperature variation of the in-flight particles, attributed to the short duration time of laser exposure. The investigation enhances our understanding of the mechanism of LACS.

Keywords cold spray · heating · in-flight particles · laser · simulation

✉ Xinkun Suo
suoxinkun@nbu.edu.cn

[1] Multidimensional Additive Manufacturing, Faculty of Mechanical Engineering and Mechanics, Ningbo University, 315211 Ningbo, People's Republic of China

[2] Department of Mechanical, Manufacturing and Biomedical Engineering, Trinity College Dublin, The University of Dublin, Parsons Building, Dublin 2, Ireland

[3] State Key Laboratory of Solidification Processing, Northwestern Polytechnical University, Xi'an 710072, People's Republic of China

Introduction

Laser-assisted cold spray (LACS), also known as supersonic laser deposition (SLD), was initially proposed by O'Neill et al. in 2006 (Ref 1). The underlying principle of LACS involves introducing a laser head into cold spraying (CS), as depicted in Fig. 1. The substrate is subjected to laser-induced heating to achieve a specific temperature, thereby effectively diminishing the critical velocity required for particle deposition. LACS is capable of producing denser and higher-performance coatings at a lower critical velocity compared with laser cladding and conventional CS, accordingly, reduces significantly processing costs and extends the range of materials (Ref 2-4).

Numerous industrial alloys have been fabricated using LACS. Kulmala et al. successfully deposited the copper coatings and the nickel coatings using LACS (Ref 5). The incorporation of laser irradiation was found to enhance coating density and improve deposition efficiency. Bray et al. prepared the titanium coatings by LACS, resulting in a significant reduction in porosity from 2 to 0.3%, an increase in deposition efficiency from 25 to 45 g/min, and a decrease in oxygen and nitrogen contents, attributed to the preheating of the substrates (Ref 6). Lupoi et al. deposited the Stellite-6 coatings using LACS, and the coating had no obvious dilution layer and exhibited better friction and wear resistance (Ref 7). Jones et al. deposited the dense tungsten coating on the molybdenum substrate using

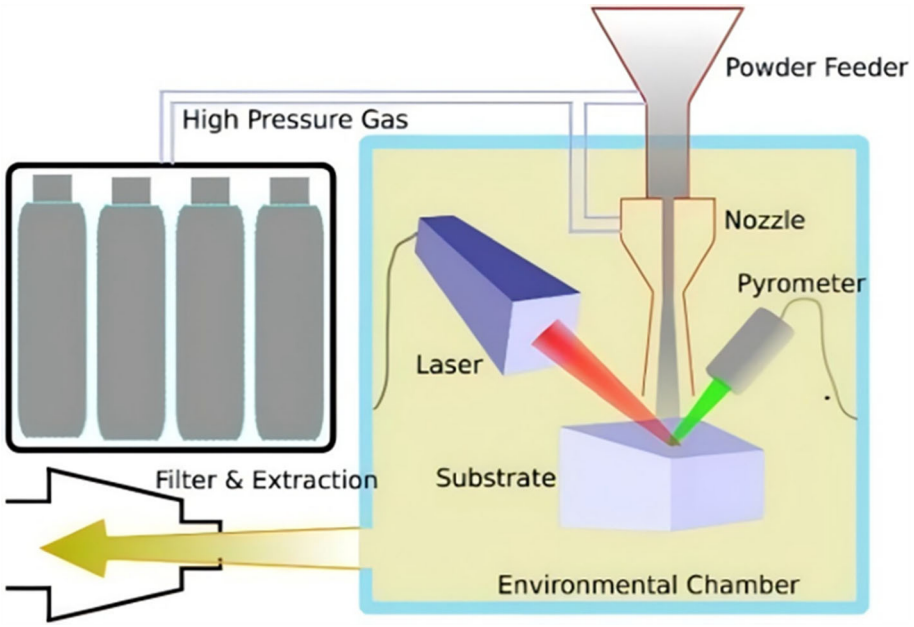

Fig. 1 Schematic diagram of laser-assisted cold spraying. Reprinted from Publication Surf. Coat. Technol., 203(19), M. Bray, A. Cockburn, W. O'Neill, The Laser-Assisted Cold Spray Process and Deposit Characterisation, p. 2851-2857, Copyright (2019), with permission from Elsevier (Ref 6)

LACS, achieving a tensile strength of 724 MPa without an evident dilution layer (Ref 8). Li et al. compared the microstructures and properties of the SS316L/WC composite coatings and Stellite-6/WC composite coatings prepared by CS and LACS. The study revealed that laser irradiation significantly improved deposition efficiency, WC concentration and interface bonding of the composite coatings (Ref 9, 10). Yao et al. and Yang et al. deposited the Ni60 coatings on the steel substrates using LACS. The coatings exhibited stable phase composition, minimal dilution rates, and exceptional friction and wear resistance (Ref 11, 12). Gorunov et al. deposited the austenitic stainless steel coatings by LACS. It was indicated that insufficient laser power could lead to coating cracking (Ref 13).

To date, two distinct parameter control strategies have been employed in LACS. One is controlling the substrate temperature through regulating the laser power in a range. Yuan et al. prepared the Stellite-6 coatings with the substrate temperature of 500 °C, 1000 °C, 1100 °C and 1200 °C (Ref 14). Story et al. prepared the Fe-Ni-Zr oxide dispersion-strengthened steel coatings through controlling the laser power in a range of 0-1084 W, while maintaining substrate temperatures at 320 °C, 650 °C, 800 °C and 950 °C (Ref 15). Barton et al. prepared the AISI 4340 steel coatings with the substrate temperature of 500 °C, 738 °C and 950 °C (Ref 16). Additionally, they prepared the oxide dispersion-strengthened $Fe_{91}Ni_8Zr_1$ coatings with the substrate temperature of 650 °C and 950 °C (Ref 17). The other strategy focuses on controlling the laser power while disregarding the substrate temperature fluctuation. Olakanmi et al. prepared the Al-12Si coatings using the laser power of 2.5 kW (Ref 18). Luo et al. prepared the Ni60-WC coatings with the laser power of 2.0 kW, 2.5 kW, 3.0 kW, 3.5 kW and 4.0 kW (Ref 19). Wang et al. prepared the molybdenum coatings with the laser power of 1.0 kW, 2.0 kW and 3.0 kW (Ref 20). Qi et al. prepared the copper coatings with the laser power ranging from 2.5 to 4.5 kW (21). Wang et al. prepared the 7075 aluminum alloy coatings with the laser power of 1.8 kW, 2.2 kW and 2.6 kW (Ref 22). Zhang et al. prepared the copper coatings with the laser power of 0.5 kW, 1.0 kW and 1.5 kW (Ref 23).

Different parameter control strategies originate from different understandings of the mechanism of LACS. It is thought that laser dominantly heats substrates for the first strategy (Ref 14-16). Consequently, the laser power is set in a range to maintain stable substrate temperature. For the second strategy, it is believed that laser heats in-flight particles and substrates (Ref 23-25), and laser power is set as a stable value. Therefore, the specific effects of the laser on the in-flight particles are in dispute. In this study, the iron and nickel coatings were deposited on the aluminum substrates with a designed experiment. The cross-sectional microstructures of the coatings were characterized, the microhardness of the coatings was measured, and the oxygen content of the coatings was measured. At the same time, multi-physical field simulation software COMSOL was used to simulate the effect of laser on the in-flight particles with different velocity and laser power. The heating mechanism of the in-flight particles in laser was discussed.

Materials and Methods

Raw Materials

The commercial iron powder (Shandong Luying New Materials Technology Co., Ltd., Shandong, China) and nickel powder (Jiangsu Weilali New Materials Technology Co., Ltd., Jiangsu, China) were used as feedstock. The surface morphology and size distribution of the powder were characterized using a scanning electron microscope (SEM, JCM-7000, JEOL, Japan) and a particle size analyzer (S3500-special, Microtrac, Montgomeryville, USA), respectively. The iron particles presented irregular morphology (Fig. 2a), with a particle size range of 30-80 μm and an average value of 45.6 μm (Fig. 2b). The nickel particles presented spherical morphology (Fig. 2c), with a particle size range of 30-80 μm and an average value of 36.4 μm (Fig. 2d). Aluminum plates (Ningbo Dongtai Metal Products Co., Ltd., Ningbo, China) were used as the substrates and polished to a mirror surface.

Coating Fabrication

The schematic sketch of the experiment is shown in Fig. 3 (Ref 26). The CS nozzle was perpendicular to the substrate, while the laser was parallel to the substrate. The distance from the spraying gun to the sample surface was 30 mm. The laser beam was set at 15 mm above the substrate, ensuring that the laser cannot heat the deposited particles. During the spraying, the nozzle and laser were fixed, while the substrate was mobile.

The coatings were prepared using a self-developed CS equipment integrated with a flat-top laser (Suzhou Leiji Laser Technology Co., Ltd., Jiangsu, China). The dimensions of the nozzle are shown in Table 1. The laser beam size was 3 mm × 3 mm, with maximum power of 6 kW and a wavelength of 1064 nm. 6 kW laser power was employed to ensure the induction of observable changes. Nitrogen was used as a process gas with pressure of 4 MPa. The temperature was set at 600 °C for the iron coatings and 700 °C for the nickel coatings. The traversing speed of the substrate was 100 mm/s. Control experiments without laser irradiation were conducted for robust comparison. The detailed process parameters are shown in Table 2.

Microstructural Characterization

The samples were taken from the central part of the prepared coatings. The iron coatings were etched using an etching solution with 90 ml HCl and 1 ml HNO_3, and the nickel coatings were etched using an etching solution with 50 ml HCl, 25 ml HNO_3 and 25 ml H_2O. The cross-sectional microstructures of the coatings were characterized using a scanning electron microscope (SEM, JCM-7000, JEOL, Japan). The porosity of the samples was calculated using image analysis software ImageJ (version 1.8.0). The microhardness of the samples was measured using a Vickers indentation tester with a load of 100 g for 15 s. An oxygen, nitrogen, and hydrogen analyzer (ONH Analyzer,

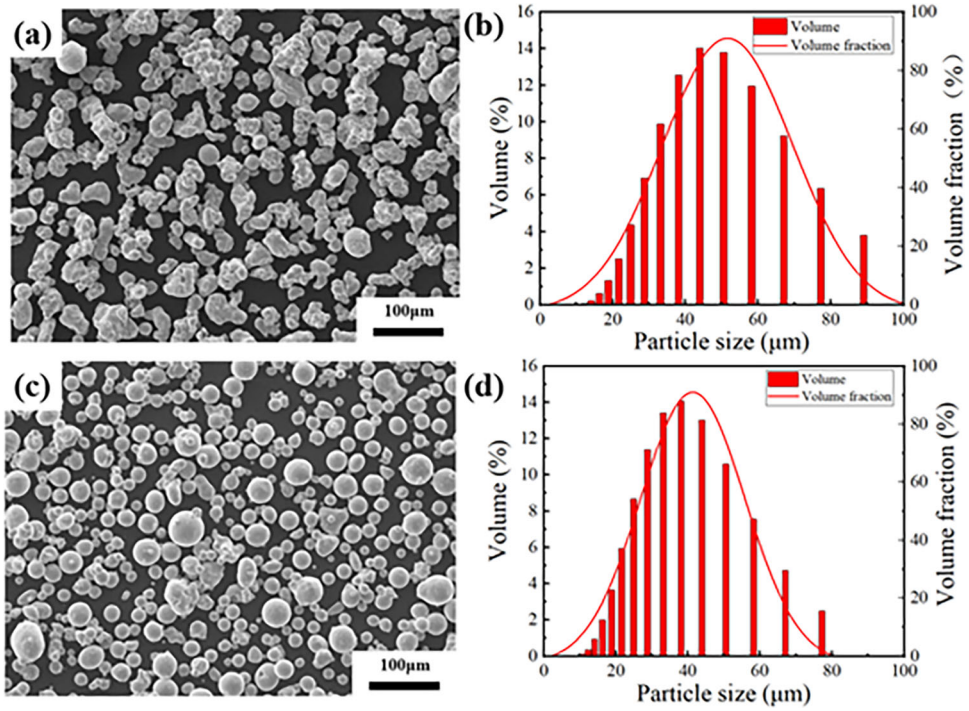

Fig. 2 Surface morphology (a) and size distribution (b) of iron powder, surface morphology (c) and size distribution (d) of nickel powder

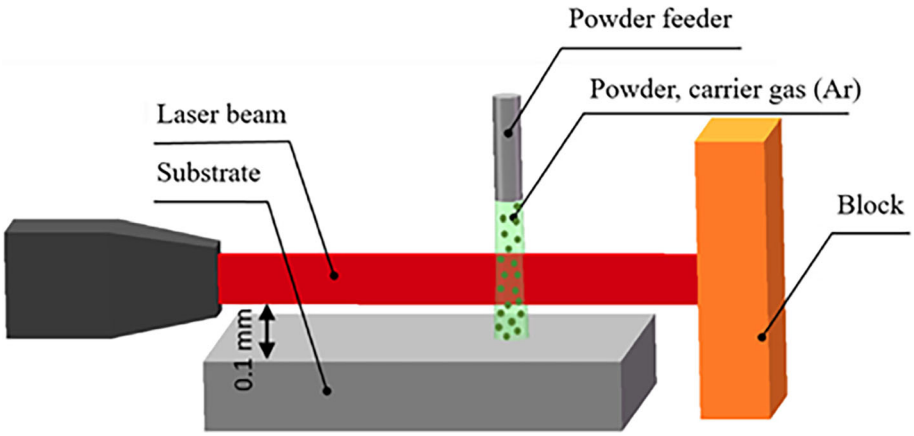

Fig. 3 The schematic sketch of the experiment process. Used under a CC BY-NC-ND 4.0 license: https://creativecommons.org/licenses/by-nc-nd/4.0/ (Ref 26)

Table 1 The dimensions of the nozzle

Inlet, mm	Convergent length, mm	Throat, mm	Expansion length, mm	Outlet, mm
10	43	1.5	200	3.5

Table 2 The process parameters of experiments

Samples	Laser power, kW	Gas temperature, °C	Gas pressure, MPa	Spray distance, mm
Fe	0	600	4	30
Fe with laser	6	600	4	30
Ni	0	700	4	30
Ni with laser	6	700	4	30

ONH836, LECO, United States) was used to measure the oxygen content of the coatings.

Numerical Simulations

Ansys (version 2021R1) was employed to calculate the velocity and temperature of the in-flight particles before entering the laser. The details of the simulation can be found in the previous study (Ref 27). The initial velocity and temperature of the iron particles entering laser irradiation were 567 m/s and 689 K. The initial velocity and temperature of the nickel particles entering laser irradiation were 561 m/s and 769 K. The heating time of the iron and nickel particles in laser was 5.3 μs and 5.4 μs, respectively. The interaction between the laser and the in-flight particles was numerically simulated using COMSOL Multiphysics (version 6.0). Radiative transfer mode (RTM) was employed to calculate the energy absorption and reflection of the particles. Ray convergence verification was performed to ensure data reliability, and the number of rays was set to 1,000,000 and 800,000 for the iron particles and nickel particles, respectively. The finite element module (FEM) in COMSOL was employed to compute the heat transfer and localized thermal effects within the particles. The material parameters were extracted from the COMSOL database (Ref 28). Different simulation parameters, including particle velocity and laser power, were examined to evaluate the robustness of the results. The particle velocity varied within the range of 300-1000 m/s, while the laser power was regulated in a range of 0-6 kW.

Results

The cross-sectional microstructures of the coatings with different laser power are shown in Fig. 4. The coatings exhibited dense microstructures with minimal porosity observable. The porosity of the CS iron coatings was $4.83 \pm 0.81\%$, which slightly decreased slightly to $4.74 \pm 0.29\%$ with the irradiation of laser. Similarly, the porosity of the nickel coatings with and without laser irradiation was $3.85 \pm 0.11\%$ and $4.03 \pm 0.17\%$, respectively. Moreover, the boundaries of the particles can be clearly observed in the iron and nickel coatings after etching. The flattening ratio of the iron particles prepared by CS was $0.29 \pm 0.02\%$, and it remained at $0.29 \pm 0.01\%$ with the irradiation of the laser. The flattening ratio of the nickel particles with and without laser irradiation was $0.33 \pm 0.03\%$ and $0.33 \pm 0.04\%$, respectively. The effects of laser irradiation on the porosity and flattening ratios of the coatings are shown in Fig. 5. It can be inferred that the microstructures of CS coatings exhibit

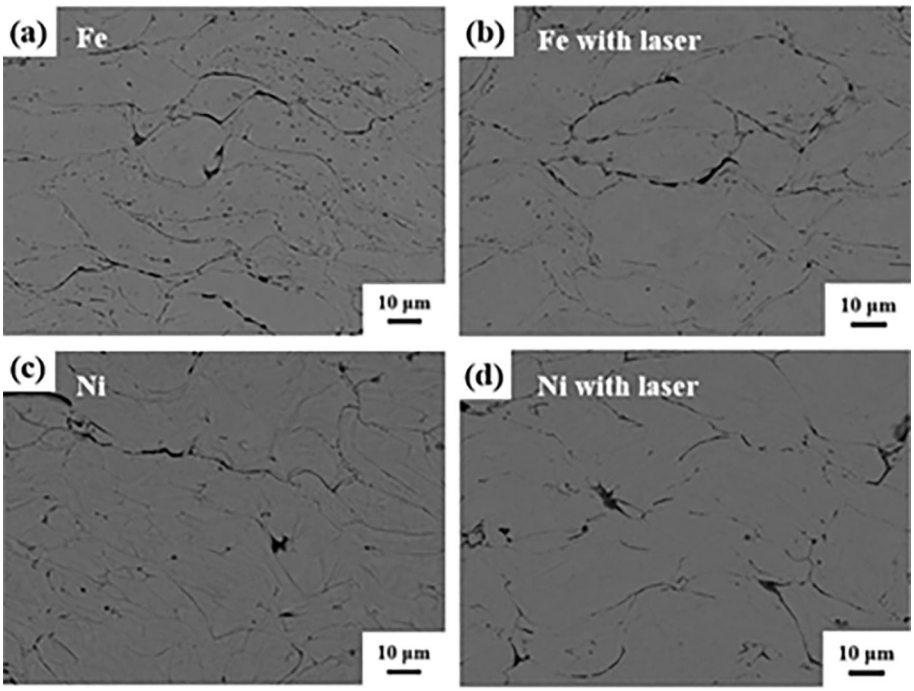

Fig. 4 The etched cross-sectional microstructures of iron coatings (a, b) and nickel coatings (c, d)

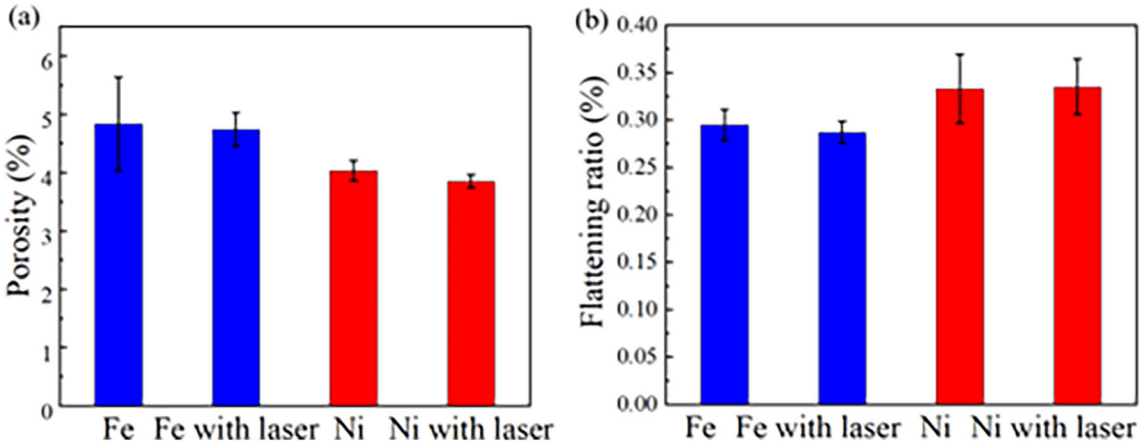

Fig. 5 The porosity (a) and flattening ratios (b) of the coatings

no significant correlation with the heating behavior of in-flight particles in laser.

Figure 6 shows the oxygen content of the coatings as a function of the laser irradiation. The oxygen content of the iron coatings prepared by CS was 2450 ± 30 ppm, which increased to 2700 ± 20 ppm with the laser irradiation. The oxygen content of nickel coatings prepared through CS was 380 ± 10 ppm, and it slightly decreased to 330 ± 30 ppm with laser irradiation. The oxygen content of the coatings also has no significant variation with the irradiation of laser.

The microhardness of the coatings with different laser power is shown in Fig.7. The microhardness of the iron coatings reduced from 166 ± 12 to 161 ± 8 HV with the irradiation of laser. However, the microhardness of the nickel coatings almost unchanged. The microhardness of the nickel coatings decreased from 194 ± 10 to193 ± 18 HV with the irradiation of laser. It can be deduced that the laser irradiation did not have a significant impact on the microhardness of the coatings.

Figure 8 shows the temperature gradient diagram of the in-flight particles with irradiation of laser. It was found that the position irradiated by the laser presented the highest temperature, and then the local temperature reduced layer by layer. The highest and lowest temperature for the same iron particle was 765 K and 693 K, respectively, and the highest and lowest temperature for the same nickel particle was 837 K and 773 K, respectively, proving that the

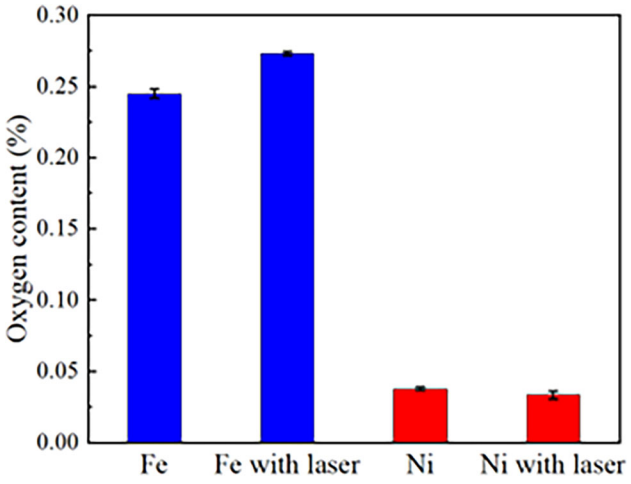

Fig. 6 The oxygen content of the coatings

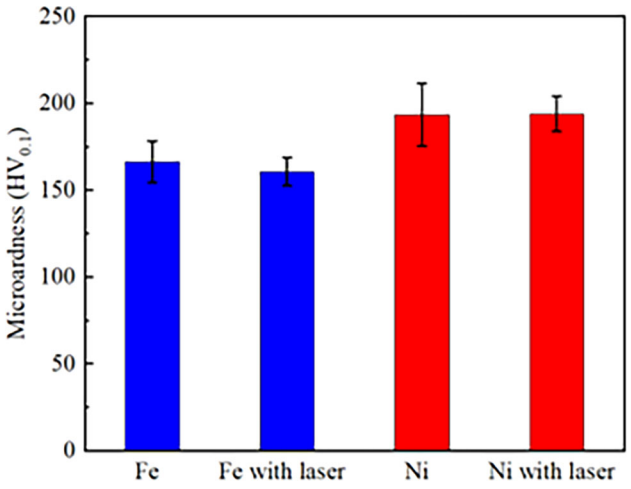

Fig. 7 The microhardness of the coatings

temperature was uneven distributed in one particle during laser irradiation.

Figure 9 shows the evolution of the particle average temperature as functions of particle velocity and laser power. The temperature of the in-flight particles increased slightly with the laser irradiation of 6 kW, and the increasing range of temperature decreased with the increase of the particle velocity (Fig. 9a). The in-flight Ni particle temperature increased from 770 to 797 K with the particle velocity of 300 m/s. As the particle velocity increased to 1000 m/s, the in-flight Ni particle temperature increased from 771 to 778 K. Figure 9(b) shows the evolution of the in-flight particle temperature as a function of laser power at 500 m/s. It is found that the temperature of the Fe particles slightly increased from 689 to 704 K as the laser power increased from 0 to 6 kW. The temperature of the Ni particles slightly increased from 769 to 784 K as the laser power increased from 0 to 6 kW. It can be deduced that the influence of laser power on the in-flight particle temperature was extremely subtle.

Discussion

The experiment results on the porosity, flattening ratios, oxygen content, and microhardness of the coatings are summarized in Table 3. Laser irradiation of the in-flight particles had no significant effect on the microstructures and properties of the coatings. It is deduced that the effect of laser in LACS is to heat the substrates and deposited particles. Zhou et al. compared the porosity of the CuCrZr coatings fabricated by CS and LACS, reporting that the porosity of the coatings produced by LACS decreased from

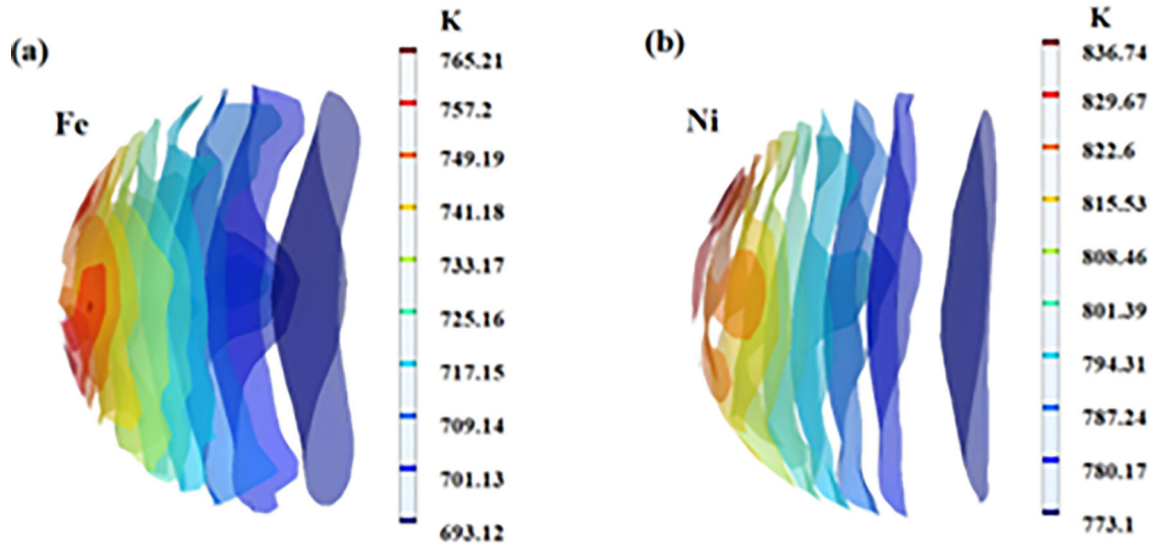

Fig. 8 The temperature gradient of the Fe particle (a) and Ni particle (b) irradiated by laser

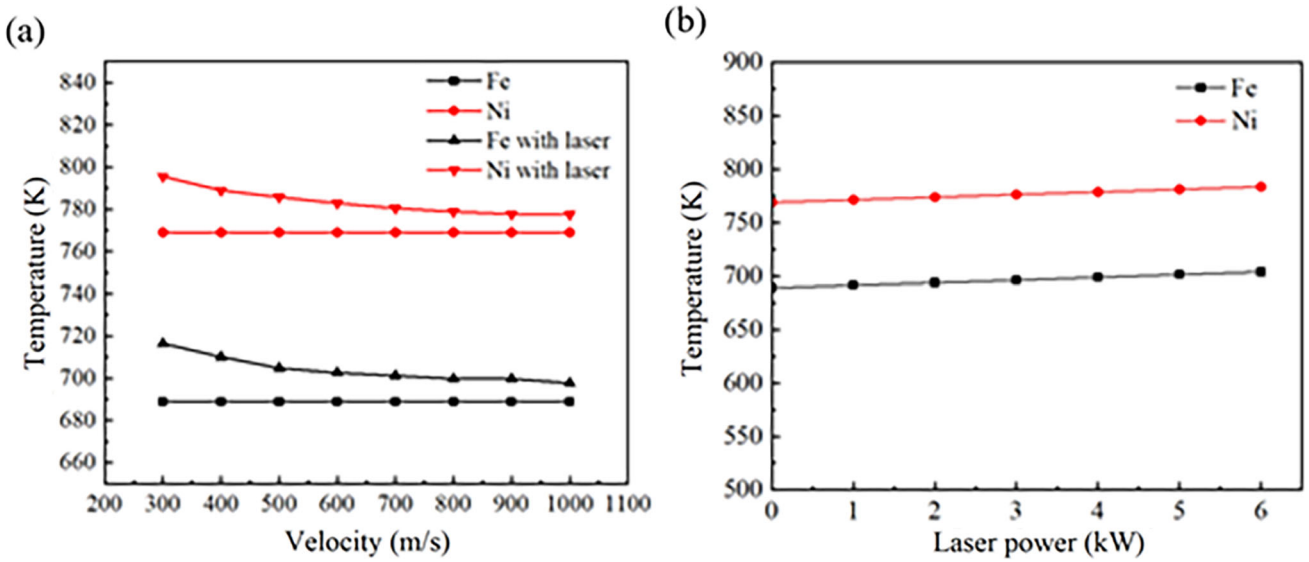

Fig. 9 The particle temperature as functions of the particle velocity (a) and laser power (b)

Table 3 Experiment and simulation results

	Porosity, %	Flattening ratio, %	Oxygen content, ppm	Microhardness, $HV_{0.1}$	Simulated $T_{particle}$, K
Fe	4.83 ± 0.81	0.29 ± 0.02	2450 ± 30	166.24 ± 12.02	688
Fe with laser	4.74 ± 0.29	0.29 ± 0.01	2700 ± 20	160.50 ± 8.07	704
Ni	4.03 ± 0.17	0.33 ± 0.04	380 ± 10	193.42 ± 18.01	769
Ni with laser	3.85 ± 0.11	0.33 ± 0.03	330 ± 30	193.88 ± 10.11	783

1.1 to 0.16% compared with those produced by CS (Ref 29). Wang et al. reported that the porosity of the 7075 aluminum coatings prepared using LACS with the laser power of 2.2 kW was approximately 0.1%, which was 20 times lower than the porosity of the coatings produced by CS (Ref 22). The decrease in coating porosity in LACS was attributed to the increase of the coating temperature, under the action of laser irradiation. Barton et al. found that the particle deformation in the coatings prepared by LACS with the substrate temperature of 650 °C was more apparent compared to those in the coatings produced by CS, which was attributed to heat conduction from the laser heated coatings to the impact particles during deposition (Ref 17). At the same time, it was observed that the oxygen content of the coatings prepared by LACS significantly increased compared with that of the CS coatings, which can also be attributed to higher coating temperature under the action of laser irradiation. Story et al. reported that the microhardness of the Fe-Ni-Zr coatings prepared by LACS was 280 ± 6 HV, meanwhile that produced by CS was 455 ± 11 HV under the same spray parameters (Ref 15). Barton et al. prepared the 4340 steel coatings using LACS and CS (Ref 16). The microhardness of the CS coating was 569 HV, and that decreased to 476 HV as the substrate temperature was 500 °C with laser heating. The decrease in coating microhardness was attributed to annealing under the action of laser irradiation (Ref 30). Furthermore, the simulation results also verified the above analysis, in which the temperature of the iron and nickel particles only increased by 16 K and 14 K with laser irradiation to 6 kW. Therefore, heating and softening effects for substrates play a dominant role in LACS, rather than in-flight particles.

Conclusions

The effects of laser on the in-flight particles and coatings were investigated through the designed experiments and simulations. Main conclusions can be drawn.

1. The laser irradiation on in-flight particles did not significantly alter the porosity, flattening ratios, oxygen content and microhardness of the coatings.
2. The temperature of the in-flight particles increased slightly with the laser irradiation, and the temperature increasing range decreased with the increase of the

particle velocity. The influence of laser power on the in-flight particle temperature was extremely subtle. The temperature was unevenly distributed in one particle during laser irradiation.

Acknowledgments This work was supported by National Natural Science Foundation of China (52171072).

References

1. M. Bray, S. Celotto, and W. O'Neill, Development of a laser assisted material spraying process. In: *Proceedings of the International Congress on Applications of Laser and Electro-Optics (ICALEO 06)*, Laser Institute of America, Arizona, USA, 2006, pp. 103-109.
2. J.H. Yao, Z.H. Li, B. Li, and L.J. Yang, Characteristics and Bonding Behavior of Stellite6 Alloy Coating Processed with Supersonic Laser Deposition, *J. Alloys Compd.*, 2016, **661**, p 526-534.
3. A.I. Gorunov, Features of Coatings Obtained by Supersonic Laser Deposition, *J. Therm. Spray Technol.*, 2018, **27**(7), p 1194-1203.
4. D.J. Barton, V.S. Bhattiprolu, B.C. Hornbuckle, C.M. Batali, K.A. Darling, G.B. Thompson, and L.N. Brewer, Residual Stress Generation in Laser-Assisted Cold Spray Deposition of Oxide Dispersion Strengthened $Fe_{91}Ni_8Zr_1$, *J. Therm. Spray Technol.*, 2020, **29**, p 1550-1563.
5. M. Kulmala and P. Vuoristo, Influence of Process Conditions in Laser-Assisted Low-Pressure Cold Spraying, *Surf. Coat. Technol.*, 2008, **202**(18), p 4503-4508.
6. M. Bray, A. Cockburn, and W. O'Neill, The Laser-Assisted Cold Spray Process and Deposit Characterisation, *Surf. Coat. Technol.*, 2019, **203**(19), p 2851-2857.
7. R. Lupoi, A. Cockburn, M. Sparkes, and F. Luo, Hardfacing Steel with Nanostructured Coatings of Stellite-6 by Supersonic Laser Deposition, *Light Sci. Appl.*, 2012, **1**(5), p 10.
8. M. Jones, R. Lupoi, A. Cockburn, M. Sparkes, and W. O'Neill, Solid-State Manufacturing of Tungsten Deposits onto Molybdenum Substrates with Supersonic Laser Deposition, *Mater. Lett.*, 2014, **134**, p 295-297.
9. B. Li, J.H. Yao, Q. Zhang, Z. Li, and L. Yang, Microstructure and Tribological Performance of Tungsten Carbide Reinforced Stainless Steel Composite Coatings by Supersonic Laser Deposition, *Surf. Coat. Technol.*, 2015, **275**, p 58-68.
10. B. Li, Y. Jin, J.H. Yao, Z.H. Li, and Q.L. Zhang, Solid-state Fabrication of WC_p-Reinforced Stellite-6 Composite Coatings with Supersonic Laser Deposition, *Surf. Coat. Technol.*, 2017, **321**, p 386-396.
11. J. Yao, L. Yang, B. Li, and Z. Li, Characteristics and Performance of Hard Ni60 Alloy Coating Produced with Supersonic Laser Deposition Technique, *Mater. Design*, 2015, **83**, p 26-35.
12. L. Yang, B. Li, J.H. Yao, and Z. Li, Effects of Diamond Size on the Deposition Characteristic and Tribological Behavior of Diamond/Ni60 Composite Coating Prepared by Supersonic Laser Deposition, *Diam. Relat. Mater.*, 2015, **58**, p 139-148.
13. A.I. Gorunov and A.K. Gilmutdinov, Investigation of Coatings of Austenitic Steels Produced by Supersonic Laser Deposition, *Opt. Laser Technol.*, 2017, **88**, p 157-165.
14. L.J. Yuan and J.H. Yao, Deposition Behavior at Different Substrate Temperatures by Using Supersonic Laser Deposition, *J. Iron. Steel Res. Int.*, 2013, **20**(10), p 87-93.
15. W.A. Story, D.J. Barton, B.C. Hornbuckle, K.A. Darling, G.B. Thompson, and L.N. Brewer, Laser Assisted Cold Spray of Fe-Ni-Zr Oxide Dispersion Strengthened Steel, *Materialia*, 2018, **3**, p 239-242.
16. D.J. Barton, V.S. Bhattiprolu, G.B. Thompson, and L.N. Brewer, Laser Assisted Cold Spray of AISI 4340 Steel, *Surf. Coat. Technol.*, 2020, **400**, p 126218.
17. D.J. Barton, B.C. Hornbuckle, K.A. Darling, L.N. Brewer, and G.B. Thompson, Influence of Surface Temperature in the Laser Assisted Cold Spray Deposition of Sequential Oxide Dispersion Strengthened Layers: Microstructure and Hardness, *Mater. Sci. Eng. A*, 2021, **811**, p 141027.
18. E.O. Olakanmi, M. Tlotleng, C. Meacock, S. Pityana, and M. Doyoyo, Deposition Mechanism and Microstructure of Laser-Assisted Cold-Sprayed (LACS) Al-12 wt.% Si Coatings: Effects of Laser Power, *Jom*, 2013, **65**, p 776-783.
19. F. Luo, A. Cockburn, M. Sparkes, R. Lupoi, Z.J. Chen, W. O'Neill, J.H. Yao, and R. Liu, Performance Characterization of Ni60-WC Coating on Steel Processed with Supersonic Laser Deposition, *Def. Technol.*, 2015, **11**(1), p 35-47.
20. S. Wang, L. Cui, G. Liu, J. Hao, X. Wang, and E. Hao, Effects of Laser Powers on the Microstructure and Wear Resistance of Molybdenum Coatings Prepared by Supersonic Laser Deposition, *Surf. Coat. Technol.*, 2023, **453**, p 129142.
21. Z. Qi, Y. Li, X. Chu, Y.M. Yan, and Y. Long, Effect of Laser Power on Microstructure and Properties of Laser Assisted Cold Sprayed Copper Coatings on Steel, *Surf. Coat. Technol.*, 2024, **477**, p 130308.
22. K. Wang, L. Zhao, T. Mao, X. Cui, J. Wang, and T.Y. Xiong, Effect of Laser Lower on the Microstructure and Mechanical Properties of Laser-assisted Cold Sprayed 7075 Aluminum Alloy Deposits, *Mater. Sci. Eng. A*, 2023, **879**, p 145224.
23. Q.L. Zhang, Y.Y. Chen, B. Li, C.Y. Wang, L. Wu, and J.H. Yao, Tribological Behavior of Ti-Coated Diamond/Copper Composite Coating Fabricated via Supersonic Laser Deposition, *Lubricants*, 2023, **11**(5), p 216.
24. F. Luo, A. Cockburn, R. Lupoi, M. Sparkes, and W. O'Neill, Performance Comparison of Stellite6® Deposited on Steel Using Supersonic Laser Deposition and Laser Cladding, *Surf. Coat. Technol.*, 2012, **212**, p 119-127.
25. F. Luo, L. Rocco, C. Andrew, S. Martin, and J.H. Yao, Characteristics of Stellite6 Deposited by Supersonic Laser Deposition under Optimized Parameters, *J. Iron. Steel Res. Int.*, 2013, **20**(2), p 52-57.
26. X.Y. Ye, J.S. Wang, Q.H. Ying, M.P. Planche, H.L. Liao, and X.K. Suo, Melting Behavior of In-flight Particles in Ultra-high Speed Laser Cladding, *J. Mater. Res. Technol.*, 2023, **24**, p 7047-7057.
27. X.K. Suo, T.K. Liu, W.Y. Li, Q.L. Suo, M.P. Planche, and H.L. Liao, Numerical Study on the Effect of Nozzle Dimension on Particle Distribution in Cold Spraying, *Surf. Coat. Technol.*, 2013, **220**, p 107-111.
28. F. Wirth and K. Wegener, A Physical Modeling and Predictive Simulation of the Laser Cladding Process, *Addit. Manuf.*, 2018, **22**, p 307-319.
29. J. Zhou, P.Y. Diao, Z.W. Qi, F. Wang, S.S. Wu, X. Chu, L. Yu, B.W. Lu, and Y.C. Xie, Microstructure, Mechanical Properties, and Tribological Properties of Laser Assisted Cold Sprayed CuCrZr Coatings: Influences of Laser Power and Laser Position, *J. Alloys Compd.*, 2023, **968**, p 172151.
30. Q. Wang, N. Li, L. Zhou, W. Niu, P. Han, X. Pan, Y. Han, P. Song, and N. Hu, Microstructure and Fatigue Performance of Hard Al Alloy Repaired by Supersonic Laser Deposition with Laser Shock Peening Treatment, *Mater. Charact.*, 2023, **200**, p 112827.